The 9th European Congress on Computational Methods in Applied Sciences and Engineering
ECCOMAS Congress 2024
3–7 June 2024, Lisboa, Portugal

EFFICIENT AND ROBUST IMPLICIT SOLVERS FOR UNSTEADY FLOW PROBLEMS USING HARMONIC BALANCE

Christian Frey[1], **Graham Ashcroft**[1] **and Jan Backhaus**[1]

[1] Institute of Propulsion Technology,
German Aerospace Center (DLR)
Linder Höhe, 51147 Cologne
Germany
christian.frey@dlr.de, graham.ashcroft@dlr.de, jan.backhaus@dlr.de

Key words: harmonic balance, turbomachinery, CFD, implicit solver, pseudotime marching

Summary.

The simulation of time-periodic unsteady flows is a central problem in aeronautical applications, especially in turbomachinery. The so-called *harmonic balance* (HB) method which uses a spectral discretisation of the time derivative has been shown to be a highly efficient approach for applications in unsteady aerodynamics and nonlinear aeroelasticity. Unlike linearised frequency-domain methods, HB takes the nonlinear interaction between harmonics into account. In contrast to other disciplines (e.g. electrical circuit analysis or structural dynamics), all HB solvers in Computational Fluid Dynamics (CFD) seem to use pseudotime stepping, thereby adopting the traditional approach to achieve steady solutions. In the authors' experience, HB together with pseudotime stepping can give unsteady solutions of high accuracy at moderate costs, provided the solver converges. There are, however, occasionally configurations where, at least for some operating conditions, it seems extremely hard to achieved converged HB solutions, which raises the question of the optimal solution technique.

In this paper, we give a physical motivation for pseudotime stepping. We show that, even for highly nonlinear problems, pseudotime marching HB solvers inherit important properties from the standard time-integration approach. Roughly speaking, we show that along certain lines in the pseudotime-time plane the pseudotime HB solution corresponds to a discrete solution of the original ordinary differential equation. This shows that, given sufficiently many harmonics and small pseudotime steps, the HB solver should converge to asymptotically periodic solutions provided the initial solution is appropriate. On the other hand, we see that self-sustained flow instabilities can prevent the HB solver from converging. We illustrate our results by means of the van der Pol oscillator as well as unsteady flow problems for a NACA profile.

1 HARMONIC BALANCE

The harmonic balance approach was first introduced in CFD by Hall et al. [11]. Whereas Hall et al. cast the harmonic balance equation in the time-domain, the harmonic balance solver implemented by the authors is formulated in the frequency domain [7, 6]. Both approaches, however, rely on the alternating time-frequency domain approach which uses a discrete Fourier

transform in order to compute the temporal derivative in the frequency domain while the nonlinear spatial operators are computed in the time domain. For a review of the different harmonic balance approaches the reader is referred to the work of Gilmore and Steer [9, 10].

The harmonic balance equation for the ordinary differential equation (ODE)

$$\partial_t q + R(q) = 0, \tag{1}$$

is

$$R^{\mathrm{HB}}(\widehat{q}) = 0, \quad R_k^{\mathrm{HB}} = \mathbf{i}k\omega\widehat{q}_k + \widehat{R(q)}_k, \quad q = F^{\mathrm{inv}}\widehat{q}. \tag{2}$$

where the harmonic balance residual R^{HB} is the vector whose k-th component is R_k^{HB}. The Fourier coefficients of the flow residuals are computed using the discrete Fourier transform, the corresponding matrix of which is denoted by F. F is a pseudoinverse of F^{inv}, the matrix that corresponds to the inverse discrete Fourier transform. Let K be the number of higher harmonics and $N \geq 2K+1$ the number of sampling points t_n, $n = 0, ..., N-1$. Then,

$$q_n = \mathrm{Re}\sum_{k=0}^{K} \widehat{q}_k e^{\mathbf{i}\omega_k t_n} = F_{nk}^{\mathrm{inv}}\widehat{q}_k. \tag{3}$$

In the following, we assume that the frequencies are $\omega_k = k\omega$, for $k = 0, ..., K$ together with uniform sampling distributed over the period $\Delta t = \frac{2\pi}{\omega}$, i.e., $t_n = n\Delta t/N$. For the simulations below $N = 4K+1$ sampling points have been used.

2 PSEUDOTIME STEPPING

Pseudotime marching the system (2) means integrating the ODE

$$\frac{\partial \widehat{q}_k}{\partial \tau} + \mathbf{i}\omega k\widehat{q}_k + \widehat{R(q)}_k = 0, \quad k = 0, ..., K. \tag{4}$$

w.r.t. τ. Note that, since R is nonlinear, the k-th harmonic of the residual R will, in general, depend on all harmonics of q which implies that Eq. (4) is a coupled system. Applying the inverse Fourier transform F^{inv} to Eq. (4) gives

$$\frac{\partial q_n}{\partial \tau} + (D_t q)_n + (\Pi_K R(q))_n = 0, \quad n = 0, ..., N-1. \tag{5}$$

Here, D_t is the spectral time derivative

$$D_t = F^{\mathrm{inv}} \begin{pmatrix} 0 & 0 & \cdots & 0 \\ 0 & \mathbf{i}\omega & \cdots & 0 \\ \vdots & \vdots & \ddots & \vdots \\ 0 & 0 & \cdots & \mathbf{i}K\omega \end{pmatrix} F, \tag{6}$$

usually encountered in time-domain formulations of harmonic balance solvers (e.g. [11]). The operator Π_K represents the modal filter onto the solution space, i.e., the flow solutions along the N sampling points which can be reconstructed from up to K higher harmonics,

$$\Pi_K = F^{\mathrm{inv}}F. \tag{7}$$

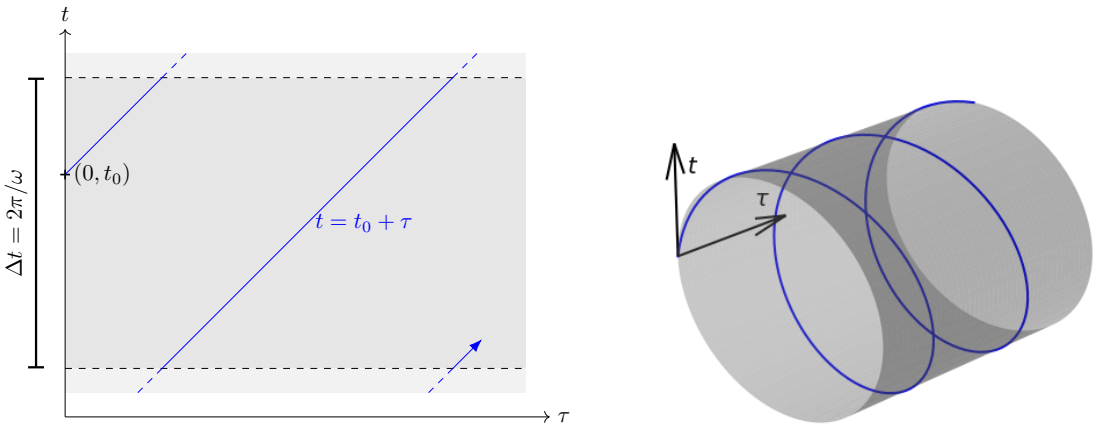

Figure 1: Integral curve of the vector field corresponding to the sum of pseudotime-time and time derivatives. Visualisations along pseudotime-time domain as plane (a) and cylinder (b).

If no oversampling is used, then $N = 2K + 1$ and Π_K is the identity operator, so Eq. (5) then takes exactly the form of the pseudotime marching of the time-domain harmonic balance (or "time-spectral") solvers, cf. [11, 21].

It follows that the pseudotime marching harmonic balance solvers, regardless of whether they are modal or nodal in time, implement a discretisation of the partial differential equation

$$\frac{\partial q}{\partial \tau} + \frac{\partial q}{\partial t} + R(t, q) = 0, \quad q(0, t) = q^0(t) \tag{8}$$

where $q(\tau, t)$ is Δt-periodic in t. $q^0(t)$ is the initial solution used to start the pseudotime solver, typically a solution to a steady problem.

We have added the time-dependence of R as, in general, the unsteadiness can be due to a relative rotation, a blade vibration or an unsteady inhomogeneous boundary condition. Eq. (8) is a transport equations in the τ-t-plane, the characteristics of which are $t = t_0 + \tau$. In Figure 1 the characteristic is plotted as a line in the planar domain

$$\{(\tau, t) \,|\, \tau \geq 0, \quad 0 \leq t \leq \Delta t\}$$

with periodic boundaries in the t-direction as well as a helix in the τ-t domain, the latter visualised as a semi-infinite cylinder.

Let q be a solution $q(\tau, t)$ to the semi-discrete system in Eq. (8), and let $\widetilde{q}_{t_0}$ be the restriction of q to one of the helices, i.e., for $t_0 \in \mathbb{R}$, let

$$\widetilde{q}_{t_0}(t) = q(t - t_0, t), \quad t \geq t_0.$$

It follows that $\widetilde{q}_{t_0}$ satisfies

$$\begin{aligned} \frac{\partial \widetilde{q}_{t_0}}{\partial t}\Big|_t &= \frac{\partial q}{\partial \tau}\Big|_{(t-t_0,t)} + \frac{\partial q}{\partial t}\Big|_{(t-t_0,t)} = \left(\frac{\partial}{\partial \tau} + \frac{\partial}{\partial t}\right) q(t - t_0, t) \\ &= -R(t, q(t - t_0, t)) = -R(t, \widetilde{q}_{t_0}(t)), \end{aligned}$$

so $\widetilde{q}_{t_0}$ is the solution to the semi-discrete URANS equation,

$$\frac{\partial \widetilde{q}_{t_0}}{\partial t} + R(t, \widetilde{q}_{t_0}(t)) = 0, \tag{9}$$

with initial value given by

$$\widetilde{q}_{t_0}(t_0) = q(0, t_0).$$

Hence, the harmonic balance solution along the characteristics $t = t_0 + \tau$ corresponds to a solution of the semi-discrete URANS equations. Assume $q^*(t)$ is a periodic solution of the URANS equations. Then the harmonic balance solutions along the helices $\widetilde{q}_{t_0}$ will approach q^* for any sufficiently close initialisation if and only if q^* is an asymptotically stable solution. Therefore, for a stable limit cycle q^* with period $2\pi/\omega_{\mathrm{lc}}$, we expect the reconstructed peudotime HB solution $F^{\mathrm{inv}}\widehat{q}$ to approach the orbit of q^*, provided the discretisation errors of the pseudotime discretisation and the spectral time derivative are small.

For a stable non-autonomous system, the limit frequency $\omega = \omega_{\mathrm{lc}}$ and the phase of the solution are dictated by the external source. For autonomous systems, however, an arbitrary time-shift for each characteristic should be expected. To analyse this consider the simple case where the non-discretised pseudotime HB problem (8) is initialized with a solution along the exact limit cycle q^*, i.e.,

$$q(0, t) = q^*(\tfrac{\omega}{\omega_{\mathrm{lc}}} t + \Delta t(t)).$$

Note that the factor $\omega/\omega_{\mathrm{lc}}$ makes the limit cycle Δt-periodic whereas the function $\Delta t(t)$ represents an arbitrary phase modulation. Then it follows that

$$q(\tau, t + \tau) = q^*(\tfrac{\omega}{\omega_{\mathrm{lc}}} t + \Delta t(t) + \tau),$$

for $\tau \geq 0$. This can be written in the form

$$q(\tau, t') = q^*(\tfrac{\omega}{\omega_{\mathrm{lc}}} t' + \Delta t(t' - \tau) + \tau(1 - \tfrac{\omega}{\omega_{\mathrm{lc}}})), \tag{10}$$

for $\tau \geq \tau_0$. The third summand term on the right-hand side corresponds to a global time shift which propagates with speed

$$\frac{dt}{d\tau} = \frac{\omega}{\omega_{\mathrm{lc}}} - 1.$$

It has been observed in the literature (see e.g. [20, 3]) that the sign of the phase difference between two pseudotime steps of some monitoring quantity can be used to deduce whether the current frequency ω is greater or smaller than the true frequency ω_{lc}. Eqn. (10) explains why such approaches are successful in the context of pseudotime stepping.

The second summand on the right-hand side of (10) shows that with the exact pseudotime integration the phase modulation, rather than disappear, will be transported along the characteristics. In addition to the frequency offset, we thus see another possible cause for the non-convergence of the HB solver. The following model problem, however, indicates that if, as in practical applications, we employ a more dissipative pseudotime integration method (such as Euler backward), then this unsteadiness is attenuated.

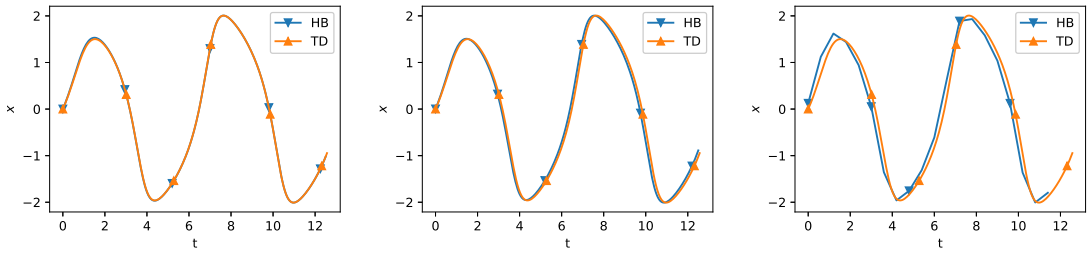

(a) Exact (b) EB, $\Delta\tau = 0.05$ (c) EB, $\Delta\tau = 0.6$

Figure 2: Comparison of the HB solutions along a helix with the time integration result during the initial phase.

Van der Pol Oscillator

To illustrate the behaviour of the pseudotime HB solver for autonomous systems, we consider the unforced van der Pol oscillator as a most simple model problem to which the harmonic balance approach and pseudotime marching can be applied. Its second-order differential equation is

$$\ddot{x} - \mu(1 - x^2)\dot{x} + x = 0. \tag{11}$$

As is well-known, the van der Pol oscillator has a limit cycle with amplitude in the order of 2 and angular frequency in the order of 1 which depend on the value of μ. Note that the van der Pol oscillator has been used for the study of the impact of the alternating frequency-time domain approach by Liu et al. [16]. Here, we will illustrate the pseudotime transient behaviour by means of this model equation.

First, we write (11) as a first order system with two degrees of freedom

$$\dot{q} + R(q) = 0, \quad R(q) = \begin{pmatrix} -q_2 \\ -\mu(1 - q_1^2)q_2 + q_1 \end{pmatrix}. \tag{12}$$

The authors have implemented a pseudotime solver for this equation in python, i.e., a solver which integrates (4) with respect to τ. For this purpose, we used the `odeint` method of SciPy which is a wrapper around the LSODA method for the integration of stiff and non-stiff ordinary differential equations [12]. This way we obtain a reference solution for the pseudotime integration which will be called "exact" in the following. Furthermore, a second approach was implemented which mimics typical implementations in CFD and computes, at each discrete pseudotime step the update $\Delta\widehat{q}^{(m)} = \widehat{q}^{(m+1)} - \widehat{q}^{(m)}$ by the approximate Euler backward (EB) scheme

$$\left(\frac{1}{\Delta\tau} + \frac{\partial R^{\mathrm{HB}}}{\partial \widehat{q}}\bigg|_{\widehat{q}^{(m)}}\right) \Delta\widehat{q}^{(m)} = -R^{\mathrm{HB}}(\widehat{q}^{(m)}), \tag{13}$$

with a given pseudotime step size $\Delta\tau$. In the following, μ is set to one, and the HB solver uses 13 harmonics and no oversampling, i.e., 27 sampling points. The pseudotime HB solver is initialised with sine/cosine waves of amplitude 1 for q_1 and q_2 and the angular frequency ω is set to 1 which is roughly 5% above the actual limit cycle frequency.

Figure 2 compares the initial phase of the pseudotime HB solutions along the characteristic $t = \tau$ to the physical time-integration result where the initial value equals that of the HB solver

at $t = 0$. We infer that the initial transient of the pseudotime HB solver along the characteristic matches that of a time-integration approach if the discretisation errors are negligible. For a larger pseudotime step size ($\Delta\tau = 0.6$) there is a slight deviation between the time integration result and the pseudotime HB solution.

Figure 3 shows the evolution of the HB solution between pseudotime step 700 and 780. For the exact pseudotime integration, we use $\Delta\tau = 0.05$ as a pseudotime step, so the curves in the left and middle plots correspond to equal pseudotimes. The abscissa is the physical time and is given in terms of the phase. We can see that, due to the offset between the solver frequency $\omega = 1$ and the true limit-cycle frequency $\omega_{\mathrm{lc}} \approx 0.94$, the solutions travel to the right as the pseudotime advances. Moreover, for the exact pseudotime integration we observe the above-mentioned phase modulation whereas for the approximate backward Euler solver (for both pseudotime step sizes) it has been attenuated.

Frequency Adaption

For autonomous problems, i.e., for self-excited flow instabilities, we have seen that with a sufficiently good initialisation, the pseudotime HB solution will approach

$$q(t) = q^*(\tfrac{\omega}{\omega_{\mathrm{lc}}} t + \Delta t), \tag{14}$$

and, if the phase modulation is attenuated, the local phase shift Δt is constant in t, so it is a function of τ. Using that q^* satisfies (1), we obtain

$$\frac{\partial q}{\partial t} = \frac{\omega}{\omega_{\mathrm{lc}}} \frac{\partial q^*}{\partial t}(\tfrac{\omega}{\omega_{\mathrm{lc}}} t + \Delta t_0) = -\frac{\omega}{\omega_{\mathrm{lc}}} R(q^*(\tfrac{\omega}{\omega_{\mathrm{lc}}} t + \Delta t_0)) = -\frac{\omega}{\omega_{\mathrm{lc}}} R(q(t)) \tag{15}$$

and therefore,

$$\mathbf{i}\omega \widehat{q}_1 = -\frac{\omega}{\omega_{\mathrm{lc}}} \widehat{R(q(t))} = -\frac{\omega}{\omega_{\mathrm{lc}}} (R_1^{\mathrm{HB}} - \mathbf{i}\omega \widehat{q}_1) \tag{16}$$

which implies

$$(\omega_{\mathrm{lc}} - \omega)\widehat{q}_1 = \mathbf{i} R_1^{\mathrm{HB}} \tag{17}$$

It follows that the true frequency ω_{lc} can be computed from

$$\omega_{\mathrm{lc}} = \omega + \frac{\langle \widehat{q}_1, \mathbf{i} R_1^{\mathrm{HB}} \rangle}{\|\widehat{q}_1\|^2} = \omega - \frac{\mathrm{Im}\langle \widehat{q}_1, R_1^{\mathrm{HB}} \rangle}{\|\widehat{q}_1\|^2}. \tag{18}$$

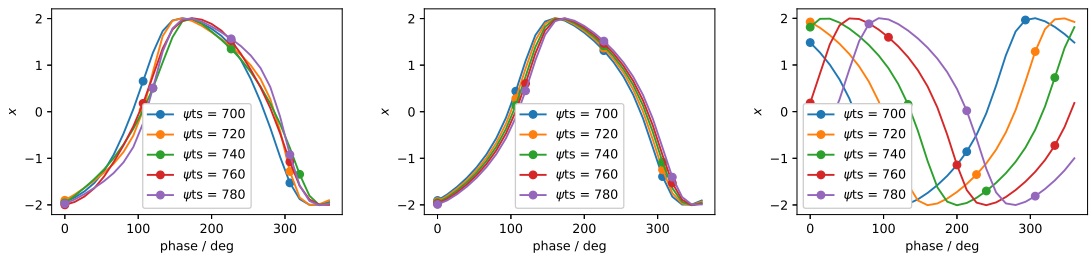

(a) Exact, $\Delta\tau = 0.05$ (b) EB, $\Delta\tau = 0.05$ (c) EB, $\Delta\tau = 0.6$

Figure 3: Pseudotime HB solutions for the exact and Euler backward pseudotime integration. Long-time behaviour of the pseudotime evolution.

Here, we assume that the complex scalar product is anti-linear in the first argument and linear in the second. This is equivalent to the so-called *gradient-based-variable-time-period* (GBVT) method of McMullen et al. [17]. Note that the same frequency correction can be obtained by determining the frequency ω^* that minimizes the first HB residual $\|R_1^{\mathrm{HB}}\|$ for the given current solution q. To see this, observe that

$$\begin{aligned}\frac{\partial}{\partial\omega^*}\|\mathbf{i}\omega^*\widehat{q}_1 + \widehat{R(q)}_1\|^2 &= 2\,\mathrm{Re}\langle\mathbf{i}\widehat{q}_1, \mathbf{i}\omega^*\widehat{q}_1 + \widehat{R(q)}_1\rangle \\ &= 2\,\mathrm{Re}\langle\widehat{q}_1, (\omega^*-\omega)\widehat{q}_1 - \mathbf{i}R_1^{\mathrm{HB}}\rangle.\end{aligned} \tag{19}$$

ω_{lc} as predicted by (18) is thus a minimizer for the first harmonic balance residual. Similar approaches to automatically determine the limit cycle frequency in the context of time-domain HB solvers have been published by Ekici and Hall [4] as well as Yao and Marques [23].

3 APPLICATION

The HB Solver in TRACE

The underlying flow solver considered here is TRACE which is DLR's inhouse flow solver for turbomachinery. TRACE has been developed for more than three decades in close cooperation with MTU Aero Engines. In the present work we employ the finite-volume spatial discretisation of the compressible RANS equations with Roe's upwind scheme [18], MUSCL extrapolation [14], and the van Albada limiter [1]. For the simulation results presented below, Wilcox' k-ω turbulence model [22] in combination with a Cauchy-Schwarz limiter is used.

The pseudotime solver discussed in this paper is formulated in the frequency domain and employs, like the steady solver, the implicit Euler method to solve Eq. (4), i.e.,

$$\widehat{q}^{(m+1)} = \widehat{q}^{(m)} + \alpha\Delta\widehat{q}^{(m)}, \tag{20}$$

where $\Delta\widehat{q}^{(m)}$ is an approximate solution to the linear equation (13). To increase the robustness of the method, a relaxation factor of $\alpha < 1$ can be applied to the approximate solution of this system. The turbulence model equations are solved in a loosely coupled way, so there are five coupled conservation equations.

To stabilize the harmonic balance solver, a temporal damping is introduced by replacing the angular frequency ω with $\widetilde{\omega} = \omega(1 - \mathbf{i}\varepsilon)$ in the definition of the spectral time derivative. ε is typically set to a value in the range of $[0, 10^{-2}]$. The simulation results below were obtained with $\varepsilon = 10^{-3}$. As is common practice the local pseudotime step size is computed from a global CFL number according to

$$\delta\tau_k = \frac{\mathrm{CFL}}{\lambda_{\max} + \omega_k},$$

where $\lambda_{\max}$ is an estimate of the maximal eigenvalue of the spatial discretization which, in turn, is computed from cell sizes and local flow conditions. Note that the pseudotime step also depends on the harmonic.

For the implicit pseudotime stepping we use an approximate Jacobian of the harmonic balance residual. First, the flow residual Jacobian corresponds to the linearisation of a spatially first order accurate upwind discretisation. Moreover, since the flow residual Jacobian is non-constant in time, the harmonic balance residual Jacobian will couple all harmonics [8]. In the standard

approach in TRACE the flow residual Jacobian is assumed to be independent of the sampling point and is simply set to the standard flow residual Jacobian evaluated at the mean flow. This decouples the harmonics in the linear system (13). In a recent effort, iteratate linear solvers have been implemented for the "fully coupled" approach [8]. The linear system can be solved with different iterative solvers which have been implemented in the a sparse linear solver library called Spliss [13].

NACA 0012 Aerofoil

The NACA 0012 aerofoil case is run at essentially incompressible conditions ($M = 0.2$) and a moderate Reynolds number per chord of $2 \cdot 10^5$. This is achieved by an appropriate reference viscosity in Sutherland's law. The mesh is relatively coarse (see Fig. 4) and farfield boundaries at a distance of about five times the chord length are used.

Blade Vibrations

Here, we consider the problem of predicting the periodic flow response when the angle of attack is $\alpha = 10°$ and the blade is vibrating with a reduced frequency

$$f_{\text{red}} = \frac{\omega c}{U_\infty} = 1.509,$$

where c is the blade chord length. The artificial eigenmode corresponds to the pitching about the profile center with a rather high amplitude of $\alpha_{\text{pitch}} = 5°$. In Fig. 5 we compare the nondimensional damping coefficient

$$\Xi = -\frac{\operatorname{Re} W_{\text{cyc}}}{\alpha_{\text{pitch}}^2 h c^2 p_{\text{dyn}}}$$

computed with the pseudotime HB solver with three harmonics. W_{cyc} denotes the work per cycle, h the blade height, p_{dyn} the farfield dynamic pressure. The plots compare the coupled

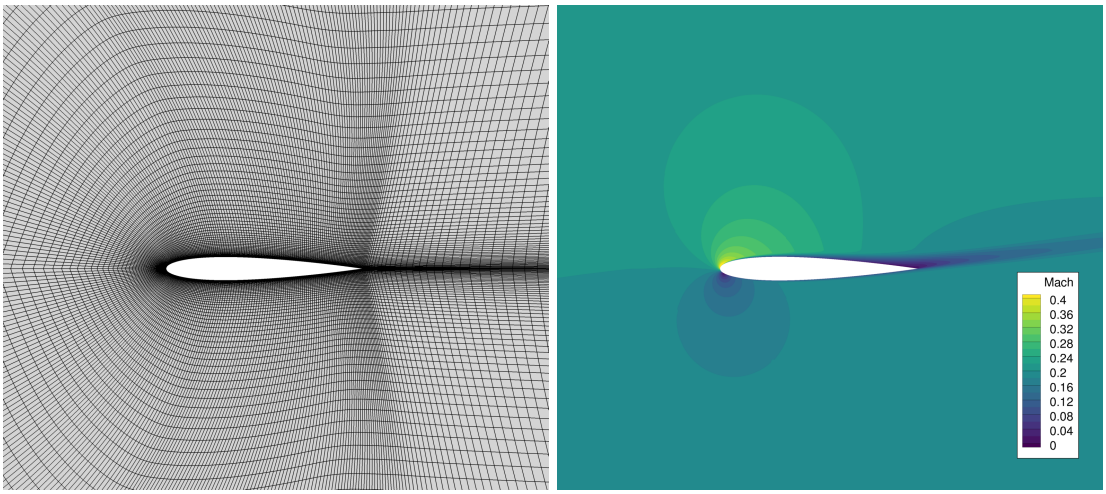

(a) Mesh (b) Mach for $\alpha = 10°$

Figure 4: NACA 0012 grid and Mach number distribution at angle of attack $\alpha = 10°$.

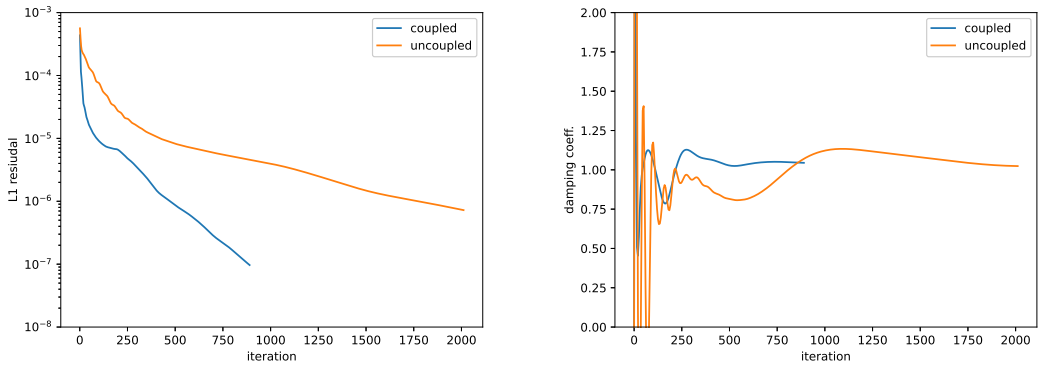

(a) Residual (b) Aerodynamic damping

Figure 5: L1 residual and damping coefficient for flutter simulation at angle of attack $\alpha = 10°$.

with the uncoupled approach for the approximate linear solver. Whereas for the uncoupled approach, we apply one SGS sweep, we use a GMRES solver with 50 iterations for the coupled system. The results show that simplifications in the linear solver may come at the expense of a reduced residual reduction per pseudotime step. As can be seen in Fig. 6, the high pitching angle causes a temporal flow separation in the profile's rear part. This problem is therefore highly nonlinear which explains why simplifications in the linear system may have a considerable impact on the solver performance. As demonstrated in [8], uncoupling the harmonics in the implicit solver, while offering considerable computational savings in many cases, can even cause severe robustness issues.

Deep Stall

To illustrate the behaviour of the HB solver for self-sustained flow instabilities, we study the flow around the NACA 0012 with an angle of attack of 40°. We compare the results obtained

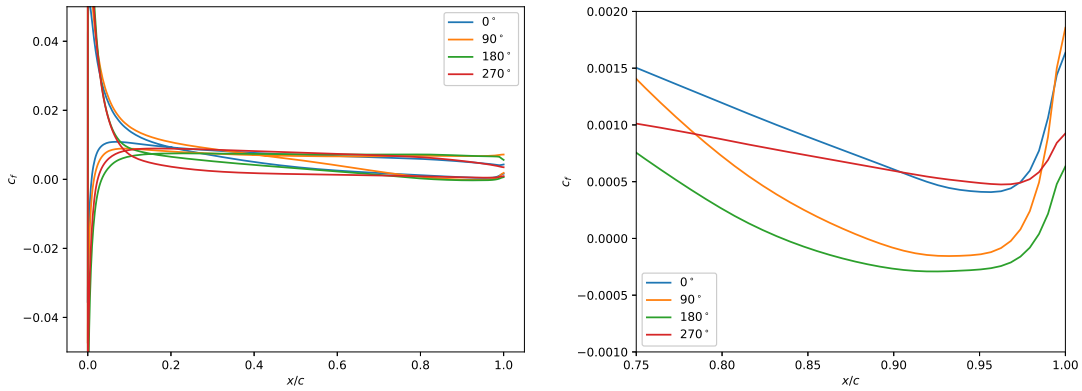

(a) Suction and pressure sides (b) Rear part of suction side

Figure 6: Skin friction at four time instants for flutter simulation at angle of attack $\alpha = 10°$.

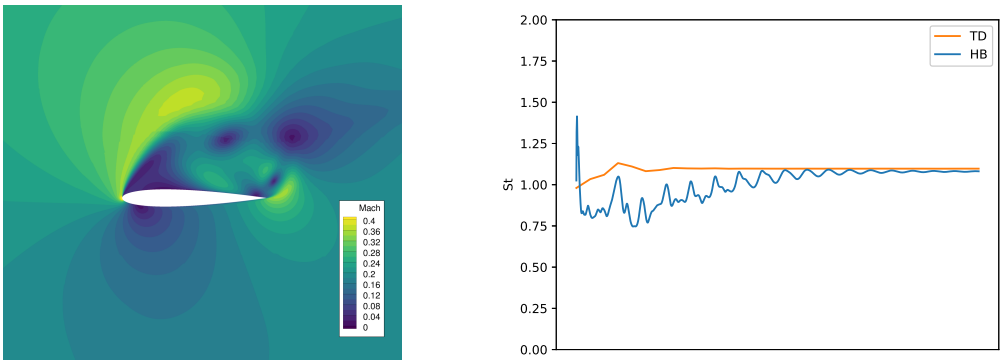

(a) Steady solver result (b) Strouhal number

Figure 7: Mach number distribution for incidence angle of 40° of non-converged steady solver (a). Convergence of Strouhal numbers as predicted by HB solver vs Runge-Kutta scheme (b).

with the HB method with seven harmonics to results of a time-marching approach. The latter uses an implicit Runge-Kutta scheme [2] with roughly 128 time steps per period. In the HB solver, we apply the frequency adaption described in (18) which we apply at each pseudotime step with an underrelaxation factor of 0.1. We initialise the HB solver with the result of a non-converged simulation with a vibrating aerofoil. During the simulation with the frequency adaption the blade is held fixed, so the system is autonomous. The Strouhal number based on the chord perpendicular to the flow $\mathrm{St} = \frac{\omega c \sin\alpha}{U}$ predicted by time-domain and HB solvers is shown in Fig. 7 and shows convergence to values which are in good agreement with each other. Figure 8 shows the vorticity at four time instants as predicted by the HB solver.

4 CONCLUSIONS AND DISCUSSION

The arguments in this work explain why pseudotime marching of the harmonic balance equations can reproduce periodic URANS solutions even in the case of strong nonlinearities. The same argument shows that neither time-integration nor pseudotime stepping HB solvers can compute unstable time-periodic solutions.

It should be emphasized, however, that our argument does not apply to temporally nonlocal boundary conditions such as some boundary conditions used for turbomachinery boundary conditions. The implementation of robust nonreflecting spectral boundary conditions, for instance,

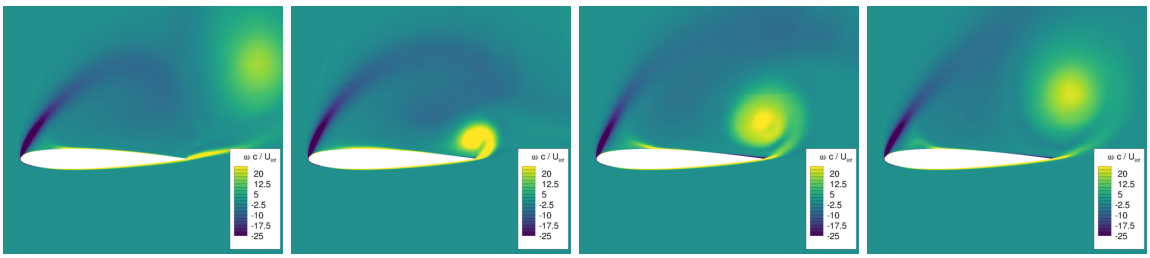

(a) 0° (b) 90° (c) 180° (d) 270°

Figure 8: Vorticity field of reconstructed HB solution for an incidence angle of 40°.

requires particular formulations which, in the authors' experience, are quite different for time integration schemes [19] than for harmonic balance methods [5]. Similar considerations can be made about the so-called *phase-lag* boundary conditions [15]. The perfect analogy between time- and frequency domain solvers, observed for the simple model problem above, cannot be expected to perfectly carry over to a turbomachinery RANS solver.

The application to the deep stall flow problem in this work, however, illustrates that the pseudotime HB solver may indeed converge to a stable limit cycle and the analysis presented should be viewed as a simple rationale why such a behaviour is expected. Summarising, the results of this paper suggest that two specific issues can cause unsatisfactory robustness or convergence speed of the pseudotime harmonic balance solver: firstly, the poor accuracy of the implicit system solver, e.g. weak iterative solvers or overly simplified system Jacobians and, secondly, the presence of an additional self-excited unsteadiness due to a flow instability.

References

[1] G. D. van Albada, B. van Leer, and W. W. Roberts Jr. "A comparative study of computational methods in cosmic gas dynamics". In: *Astron. Astrophys.* 108.1 (1982), pp. 76–84.

[2] G. Ashcroft, C. Frey, K. Heitkamp, and C. Weckmüller. "Advanced Numerical Methods for the Prediction of Tonal Noise in Turbomachinery–Part I: Implicit Runge-Kutta Schemes". In: *J. Turbomach.* 136.2 (2013), pp. 021002–021002. DOI: 10.1115/1.4023904.

[3] F. M. Besem, J. P. Thomas, R. E. Kielb, and E. H. Dowell. "An aeroelastic model for vortex-induced vibrating cylinders subject to frequency lock-in". In: *Journal of Fluids and Structures* 61 (2016), pp. 42–59. DOI: 10.1016/j.jfluidstructs.2015.10.009.

[4] K. Ekici and K. C. Hall. "Harmonic Balance Analysis of Limit Cycle Oscillations in Turbomachinery". In: *AIAA Journal* 49.7 (2011), pp. 1478–1487. DOI: 10.2514/1.J050858.

[5] C. Frey, D. Schlüß, N. Wolfrum, P. Bechlars, and M. Beck. "On the formulation of non-reflecting boundary conditions for turbomachinery configurations: Part I-Theory and implementation". In: *Proceedings of the ASME Turbo Expo*. Vol. 2C. 2020. DOI: 10.1115/GT2020-14684.

[6] C. Frey, G. Ashcroft, H.-P. Kersken, D. Schönweitz, and M. Mennicken. "Simulation of Indexing and Clocking with Harmonic Balance". In: *Int. J. Turbomach. Propuls. Power* 3.1 (2018).

[7] C. Frey, G. Ashcroft, H.-P. Kersken, and C. Voigt. "A Harmonic Balance Technique for Multistage Turbomachinery Applications". In: *ASME Turbo Expo 2014: Turbine Technical Conference and Exposition*. 45615. 2014, V02BT39A005. DOI: 10.1115/gt2014-25230.

[8] C. Frey, B. Jan, G. Ashcroft, G. Geiser, B. Winhart, and H. Stüer. "Using Pseudotime Marching for the Solution of Harmonic Balance Problems". In: *Proceedings of ASME Turbo Expo 2024 Turbomachinery Technical Conference and Exposition*. 2024. (to appear).

[9] R. J. Gilmore and M. B. Steer. "Nonlinear circuit analysis using the method of harmonic balance - A review of the art. II. Advanced concepts". In: *International Journal of Microwave and Millimeter-Wave Computer-Aided Engineering* 1.2 (1991), pp. 159–180. DOI: 10.1002/mmce.4570010205.

[10] R. J. Gilmore and M. B. Steer. "Nonlinear circuit analysis using the method of harmonic balance - A review of the art. Part I. Introductory concepts". In: *International Journal of*

Microwave and Millimeter-Wave Computer-Aided Engineering 1.1 (1991), pp. 22–37. DOI: 10.1002/mmce.4570010104.

[11] K. C. Hall, J. P. Thomas, and W. S. Clark. "Computation of Unsteady Nonlinear Flows in Cascades Using a Harmonic Balance Technique". In: *AIAA J.* 40.5 (2002), pp. 879–886. DOI: 10.2514/2.1754.

[12] A. C. Hindmarsh. "ODEPACK, a systemized collection of ODE solvers". In: *Scientific computing* (1983).

[13] O. Krzikalla, A. Rempke, A. Bleh, M. Wagner, and T. Gerhold. "Spliss: a sparse linear system solver for transparent integration of emerging HPC technologies into CFD solvers and applications". In: *STAB/DGLR Symposium 2020: New Results in Numerical and Experimental Fluid Mechanics XIII, pp 635–645*. 2021.

[14] B. van Leer. "Towards the ultimate conservative difference scheme. V. A second-order sequel to Godunov's method". In: *J. Comput. Phys.* 32.1 (1979), pp. 101–136. DOI: 10.1016/0021-9991(79)90145-1.

[15] H. D. Li and L. He. "Single-Passage Analysis of Unsteady Flows Around Vibrating Blades of a Transonic Fan Under Inlet Distortion". In: *Journal of Turbomachinery* 124.2 (2002), pp. 285–292. DOI: 10.1115/1.1450567.

[16] L. Liu, E. H. Dowell, and K. C. Hall. "A novel harmonic balance analysis for the Van Der Pol oscillator". In: *International Journal of Non-Linear Mechanics* 42.1 (2007). Nonlinear Dynamic Stability of Nonconservative Dissipative Systems, pp. 2–12. DOI: 10.1016/j.ijnonlinmec.2006.09.004.

[17] M. McMullen, A. Jameson, and J. Alonso. "Demonstration of nonlinear frequency domain methods". In: *AIAA Journal* 44.7 (2006), pp. 1428–1435. DOI: 10.2514/1.15127.

[18] P. L. Roe. "Approximate Riemann solvers, parameter vectors, and difference schemes". In: *J. Comput. Phys.* 43.2 (1981), pp. 357–372. DOI: 10.1016/0021-9991(81)90128-5.

[19] D. Schlüß and C. Frey. "Time domain implementation of a spectral non-reflecting boundary condition for unsteady turbomachinery flows". In: *24th ISABE Conference*. Proceedings of the 24th ISABE Conference. 2019.

[20] M. Spiker, R. Kielb, J. Thomas, and K. Hall. "Application of Enforced Motion to Study 2-D Cascade Lock-in Effect". In: *47th AIAA Aerospace Sciences Meeting including The New Horizons Forum and Aerospace Exposition*. 2012. DOI: 10.2514/6.2009-892.

[21] J. P. Thomas, C. H. Custer, E. H. Dowell, K. C. Hall, and C. Corre. "Compact Implementation Strategy for a Harmonic Balance Method Within Implicit Flow Solvers". In: *AIAA Journal* 51.6 (2013), pp. 1374–1381. DOI: 10.2514/1.J051823.

[22] D. C. Wilcox. "Reassessment of the Scale-Determining Equation for Advanced Turbulence Models". In: *AIAA J.* 26.11 (1988), pp. 1299–1310.

[23] W. Yao and S. Marques. "Prediction of Transonic Limit-Cycle Oscillations Using an Aeroelastic Harmonic Balance Method". In: *AIAA Journal* 53.7 (2015), pp. 2040–2051. DOI: 10.2514/1.J053565.